# A novel MRI framework for the quantification of any moment of arbitrary velocity distributions

Petter Dyverfeldt, Andreas Sigfridsson, Hans Knutsson and Tino Ebbers



This is the pre-reviewed version of the following article:

Petter Dyverfeldt, Andreas Sigfridsson, Hans Knutsson and Tino Ebbers, A novel MRI framework for the quantification of any moment of arbitrary velocity distributions, 2011, Magnetic Resonance in Medicine, (65), 3, 725-731.

which has been published in final form at:
http://dx.doi.org/10.1002/mrm.22649

# A Novel MRI Framework for the Quantification of Any Moment of Arbitrary Velocity Distributions

Petter Dyverfeldt[1-3], Andreas Sigfridsson[1,3], Hans Knutsson[3,4], Tino Ebbers[1-3]

[1] Division of Cardiovascular Medicine, Department of Medical and Health Sciences, Linköping University, Linköping, Sweden.

[2] Division of Applied Thermodynamics and Fluid Mechanics, Department of Management and Engineering, Linköping University, Linköping, Sweden.

[3] Center for Medical Image Science and Visualization (CMIV), Linköping University, Linköping, Sweden.

[4] Division of Medical Informatics, Department of Biomedical Engineering, Linköping University, Linköping, Sweden.

Running Head: Moment Framework

Word Count: 3147

Grant Sponsors: Swedish Research Council, Swedish Heart-Lung Foundation, Center for Industrial Information Technology (CENIIT).

Presented in part at the 18th Annual Meeting of ISMRM, Stockholm, Sweden, 2010.

Correspondence: Petter Dyverfeldt, Division of Cardiovascular Medicine, Department of Medical and Health Sciences, Linköping University, SE-581 83 Linköping, Sweden.
E-mail: petter.dyverfeldt@liu.se

## ABSTRACT

Magnetic resonance imaging (MRI) can measure several important hemodynamic parameters but might not yet have reached its full potential. The most common MRI method for the assessment of flow is phase-contrast MRI velocity mapping that estimates the mean velocity of a voxel. This estimation is precise only when the intravoxel velocity distribution is symmetric. The mean velocity corresponds to the first raw moment of the intravoxel velocity distribution. Here, a generalized MRI framework for the quantification of any moment of arbitrary velocity distributions is described. This framework is based on the fact that moments in the function domain (velocity space) correspond to differentials in the Fourier transform domain ($k_v$-space). For proof-of-concept, moments of realistic velocity distributions were estimated using finite difference approximations of the derivatives of the MRI signal. In addition, the framework was applied to investigate the symmetry assumption underlying phase-contrast MRI velocity mapping; we found that this assumption can substantially affect PC-MRI velocity estimates and that its significance can be reduced by increasing the velocity encoding range.

## INTRODUCTION

Magnetic resonance imaging (MRI) is a versatile tool for the non-invasive assessment of fluid motion with several important clinical and research applications (1). Most of these applications utilize the phase-contrast MRI (PC-MRI) velocity mapping technique, which provides an estimation of the mean velocity of each image voxel. The principles underlying the majority of the MRI flow quantification techniques in use date back to the work done by Hahn (2) who described the effects of motion on the phase accumulation of the transverse magnetization of spin isochromats in the presence of a magnetic field gradient. Early work in estimating flow with MRI was based on a single phase measurement (3,4); subsequent developments lead to the phase-difference technique known as PC-MRI velocity mapping (5-7). The theoretical framework underlying PC-MRI was developed by Moran *et al*. (8).

In MRI, the first order motion sensitivity of a pulse sequence is proportional to the 1st moment of the applied gradient waveform according to $k_v = \gamma M_1$, where $\gamma$ is the gyromagnetic ratio. For motion terms up to the first order, the complex-valued MRI signal of a voxel at a specific position can be written as a function of $k_v$ and the intravoxel spin velocity distribution s($v$):

$$S(k_v) = Ce^{i\varphi_{add}} \int_V s(v) e^{-ik_v \cdot v} dv \qquad [1]$$

where $C$ is a real valued constant influenced by spin density, relaxation effects, etc. and $\varphi_{add}$ is an additional phase-shift caused by factors other than spin motion, such as magnetic field inhomogeneities. In Fourier velocity encoding (8), $S(k_v)$ is sampled using a range of $k_v$ values and an inverse Fourier transform of the resulting $k_v$-space gives the distribution of spin velocities within a voxel. As a complete spatiotemporal $k$-$t$ space is required for each step in $k_v$-space, many potential applications of Fourier velocity encoding are infeasible due to prohibitive scan times. In phase-contrast MRI (PC-MRI) velocity mapping, two samples of $S(k_v)$ are acquired and an estimation of the mean of the velocity distribution within a voxel is obtained from the ratio between the phase-difference between the two MRI signals, $\Delta\varphi$, and the net motion sensitivity with which they are acquired, $\Delta k_v$:

$$V_{PC-MRI} = \left[\arg\left(S\left(k_{v_2}\right)\right) - \arg\left(S\left(k_{v_1}\right)\right)\right] / \Delta k_v = \Delta\varphi / \Delta k_v \qquad [2]$$

$\Delta k_v$ is related to the velocity encoding range (VENC) parameter according to $\Delta k_v = \pi/\text{VENC}$. Only if the intravoxel spin velocity distribution s($v$) is symmetric, $V_{\text{PC-MRI}}$ is the mean velocity of the voxel (9,10).

The standard deviation of the intravoxel spin velocity distribution (intravoxel velocity standard deviation (IVSD)) can be estimated from the magnitude relationship of two or more MRI signals (11). Under the assumption that the intravoxel velocity distribution s($v$) is Gaussian, the IVSD, $\sigma$, is obtained from (11,12)

$$\sigma = \text{sqrt}\left[\frac{2\ln\left(\left|S\left(k_{v_2}\right)\right| / \left|S\left(k_{v_1}\right)\right|\right)}{k_{v_1}^2 - k_{v_2}^2}\right], \left|k_{v_1}\right| \neq \left|k_{v_2}\right|, \quad [3]$$

The mean velocity and the IVSD correspond to the first raw moment and the square root of the second central moment, respectively, of s($v$). PC-MRI velocity and IVSD mapping estimates these moments based on assumptions about the appearance of the intravoxel spin velocity distribution.

Here, we present a generalized framework for the quantification of *any* moment of *arbitrary* spin velocity distributions. Using this framework, estimations of the mean, standard deviation, skew, and kurtosis of s($v$) are presented. The framework may improve the understanding and guide the application of current MRI motion estimation methods; this is exemplified by evaluating the implications of the symmetry assumption of PC-MRI velocity mapping.

# THEORY

## Moment Framework

Moments can be used to characterize several properties of a distribution such as its mean, standard deviation, skew, and kurtosis (see table 1). For an arbitrary distribution s($v$), the $n^{\text{th}}$ raw moment is given by

$$\mu'_n = \int_{-\infty}^{\infty} v^n s(v)\,dv \qquad [4]$$

and the $n^{\text{th}}$ central moment is given by

$$\mu_n = \int_{-\infty}^{\infty} (v - \mu'_1)^n s(v)\,dv \qquad [5]$$

where $\mu'_1$ is the mean of s($v$).

Moments in the function domain (velocity-space) correspond to differentials in the Fourier transform domain ($k_v$-space) at $k_v = 0$ (13). For the $n^{\text{th}}$ raw moment,

$$\int_{-\infty}^{\infty} v^n s(v)\,dv = i^n \frac{d^n}{dk_v^n} S(k_v)\Big|_{k_v=0} \qquad [6]$$

Thus, the moment framework describes how the different moments of the intravoxel velocity distribution s($v$) are related to the MRI signal $S(k_v)$; to obtain the $n^{\text{th}}$ (raw) moment of arbitrary intravoxel spin velocity distributions, the $n^{\text{th}}$ derivative of the MRI signal $S(k_v)$ with respect to $k_v$ at $k_v = 0$ needs to be determined. While the moment framework is not a measurement method in itself, it clarifies the prerequisites for MRI quantification of any moment of arbitrary velocity distributions. In this way, the framework may improve the understanding of current MRI moment estimation methods; this is exemplified below by addressing the problem of measuring the mean velocity of a voxel.

## Utilizing the moment framework to evaluate the mean velocity of a voxel

Consider a normalized MRI signal $T(k_v) = S(k_v)/S(0)$, where $S(0)$ corresponds to the zeroth moment of s($v$). As s($v$) is real, $S(k_v)$, and thereby also $T(k_v)$, is Hermitian. The real part of an Hermitian function, $x(k_v)$ = real($T(k_v)$), is an even function and the imaginary part, $y(k_v)$ = imag($T(k_v)$), is an odd function. By exploiting that the limit of $dx(k_v)/dk_v$ as $k_v$ approaches zero is zero, it is found that

$$\frac{dT(k_v)}{dk_v} = \frac{dx}{dk_v} + i\frac{dy}{dk_v} \rightarrow i\frac{dy}{dk_v},\ k_v \rightarrow 0 \qquad [7]$$

Thus, in the limit where $k_v$ approaches zero, the first raw moment it related only to the imaginary part of the MRI signal:

$$\mu'_1 = i\frac{dT(k_v)}{dk_v} = -\frac{dy}{dk_v} \qquad [8]$$

By also exploiting that the limits of $y(k_v)$ and $x(k_v)$ as $k_v$ approaches zero is zero and one, respectively, we get that

$$\frac{d}{dk_v}\arg(T(k_v)) = \frac{d}{dk_v}\left[\arctan\left(\frac{y}{x}\right)\right] = \frac{1}{1+(y/x)^2}\frac{x\frac{dy}{dk_v} - y\frac{dx}{dk_v}}{x^2} \rightarrow \frac{dy}{dk_v},\ k_v \rightarrow 0 \qquad [9]$$

Thus, for small values of $k_v$, the derivative of $\arg(T(k_v))$ is approximately equal to the derivative of the imaginary part of the MRI signal. If the velocity $v$ is represented by $v = V + u_{\text{dev}}$, where $V$ is the mean velocity of a voxel and $v_{\text{dev}}$ is the deviation of each spin's velocity from $V$, as done by Hamilton *et al*. (10), it is found that

$$\begin{aligned}\arg(T(k_v)) &= \arg\left(\int_{-\infty}^{\infty} s(v)e^{-ik_v v}dv\right) \\ &= \arg\left(e^{-ik_v V}\int_{-\infty}^{\infty} s(V+v_{\text{dev}})e^{-ik_v v_{\text{dev}}}dv_{\text{dev}}\right) = \\ &= -k_v V + \arg\left(\int_{-\infty}^{\infty} s(V+v_{\text{dev}})e^{-ik_v v_{\text{dev}}}dv_{\text{dev}}\right)\end{aligned} \qquad [10]$$

The widely applied PC-MRI velocity mapping method estimates the mean velocity of a voxel based on the phase difference between two measurements of $S(k_v)$, where $\Delta k_v$ is chosen so that VENC = $\pi / \Delta k_v$ is slightly higher than the peak velocity of the flow of interest. As apparent from equation 10, PC-MRI estimates the mean velocity only if the distribution $s(v)$ is symmetric, in which case the last term in equation 10 equals zero. Assuming symmetric distributions, $\arg(T(k_v))$ is linear on the interval $|k_v| < \pi / V$ and its derivative at $k_v = 0$ can be obtained from measurements made with larger $k_v$. This, in combination with the relationship between the first derivatives of $T(k_v)$ and $\arg(T(k_v))$ at $k_v = 0$ (equations 7-9), leads to equation 2 used in PC-MRI velocity mapping. Thus, equation 2 corresponds to an estimation of the mean velocity (1st raw moment) under the assumption that the distribution $s(v)$ is symmetric.

## MATERIALS AND METHODS

For proof-of-concept, estimations of the mean, standard deviation, skew, and kurtosis of s($v$) are performed based on finite difference approximations of the derivatives of $S(k_v)$. The framework may be useful in improving the understanding and guide the application of current MRI motion estimation methods; this aspect of the framework is addressed by a preliminary investigation of the significance of the symmetry assumption of PC-MRI velocity mapping.

### Moments of velocity distributions

The possibility of measuring moments of arbitrary velocity distributions was assessed by using a tailored MRI simulation approach. A virtual flow phantom consisting of numerical velocity data describing non-pulsatile flow in a straight 14.6 mm diameter circular pipe with a 75% area-reduction cosine-shaped stenosis, described previously in ref (14), was considered. The numerical velocity data were obtained using large-eddy simulations (15) and had a Reynolds number of 2000 in the unoccluded part of the phantom; flow downstream of the stenosis was studied. From these numerical velocity data, isotropic voxels (2x2x2 $mm^3$) were extracted. For each voxel, the intravoxel velocity distribution s($v$) was obtained by computing a probability density estimate of the velocities of the virtual spins. From s($v$) and the velocities of the virtual spins, $S(k_v)$ was obtained by solving equation 1 for a range of $k_v$ values. The derivatives of $S(k_v)$ at $k_v = 0$, required for accurate quantification of moments of $s(v)$, were estimated by finite differentiation. The following relations were used:

$$\mu'_1 = i\frac{d}{dk_v}\left(T(k_v)\right)\Big|_{k_v=0} \approx i\frac{T(\Delta k_v)-T(0)}{\Delta k_v} \qquad [11]$$

$$\mu'_2 = i^2\frac{d^2}{dk_v^2}\left(T(k_v)\right)\Big|_{k_v=0} \approx -\frac{T(\Delta k_v)-2T(0)+T(-\Delta k_v)}{\Delta k_v^2} \qquad [12]$$

$$\mu'_3 = i^3\frac{d^3}{dk_v^3}\left(T(k_v)\right)\Big|_{k_v=0} \approx -i\frac{T(2\Delta k_v)-3T(\Delta k_v)+3T(0)-T(-\Delta k_v)}{\Delta k_v^3} \qquad [13]$$

$$\mu'_4 = i^4\frac{d^4}{dk_v^4}\left(T(k_v)\right)\Big|_{k_v=0} \approx \frac{T(2\Delta k_v)-4T(\Delta k_v)+6T(0)-4T(-\Delta k_v)+T(-2\Delta k_v)}{\Delta k_v^4} \qquad [14]$$

where $T(k_v) = S(k_v)/S(0)$ and it is assumed that the acquisitions of $S(k_v)$ and $S(0)$ differ only in their first gradient moment, as is the case in PC-MRI where $S(k_v)$ and $S(0)$ are typically acquired in an interleaved manner. In particular, the same echo time should be used for all motion-

encoding segments. As the moments should be real, the absolute values of the estimated $\mu'_1$, $\mu'_3$, and $\mu'_4$ were used. For normalized distributions ( $\mu'_0 = 1$), such as $T(k_v)$, central and raw moments are related according to

$$\mu_n = \sum_{j=0}^{n} \binom{n}{j} (-1)^{n-j} \mu'_j \, \mu'^{\,n-j}_1 \qquad [15]$$

Using this relation, the mean, standard deviation, skew, and kurtosis of $s(v)$ (see table 1) were obtained from the estimated raw moments of $s(v)$ (equations 11-14). Note that as $S(k_v)$ is Hermitian, $S(-k_v)$ is the complex conjugate of $S(k_v)$. Thus, two measurements of $S(k_v)$ are sufficient for the estimation of the mean velocity and standard deviation, and three measurements for skew and kurtosis. Note that, by definition, the accuracy of finite difference approximations declines as the spacing $\Delta k_v$ increases. This approach to the estimation of mean, IVSD, skew, and kurtosis was investigated as a function of $\Delta k_v$. This was done both with and without noise. Gaussian distributed noise with standard deviation 0.001 was added to the real and imaginary components of $S(k_v)$. The results of the estimated mean velocity and standard deviation of $s(v)$ were compared with PC-MRI velocity (equation 2) and IVSD (equation 3) mapping, respectively.

Significance of the symmetry assumption underlying PC-MRI velocity mapping

The utility of the moment framework for improving the understanding and guide the application of current MRI motion estimation methods was tested by studying the error introduced by the symmetry assumption underlying PC-MRI velocity mapping. A square-pixel grid of PC-MRI velocity data was reconstructed in an axial slice at 1.5 diameters downstream from the stenosis of the virtual flow phantom described above. At this slice position, the flow field is characterized by a post-stenotic jet with a surrounding shear layer. The peak jet velocity was about 7 m/s. The root-mean-square error of the PC-MRI velocities and the percentage error in flow rate calculated from these velocities were determined for different VENC's and pixel sizes, as specified in table 2.

## RESULTS

The spin velocity distributions of three different voxels extracted from the numerical post-stenotic flow data, along with the modulus and argument of the corresponding MRI signals, are plotted in figure 1. The three different velocity distributions are all non-Gaussian and non-symmetric. In figure 2, finite difference approximations of the first derivative of each of the $S(k_v)$ presented in figure 1 are plotted against the spacing $\Delta k_v$; this is done both in absence and presence of noise. In absence of noise, a small $\Delta k_v$ (good approximation of the derivative) provides accurate estimates of $V$, proving the concept of the moment framework. In presence of noise, the two measurements of $S(k_v)$ at $k_v$ close to zero (high VENC) become more influenced by noise than by the small differences in $S(k_v)$, resulting in unreliable estimates. By approximating $s(v)$ as a symmetric distribution, i.e. applying PC-MRI velocity mapping, more robust estimations of $V$ can be obtained with greater $\Delta k_v$ (figure 2, right column) when $s(v)$ is not highly asymmetric. In the cases shown here, the maximum error caused by the symmetry assumption is about 5%. Note that velocity aliasing occurs when $|\Delta k_v| > \pi / V$. In PC-MRI velocity mapping, $\Delta k_v$ is typically set so that the VENC parameter ($\pi/\Delta k_v$) matches the peak velocity of the flow of interest; a higher VENC is avoided because it decreases the velocity-to-noise ratio. However, by providing a better approximation of the first derivative of $S(k_v)$, a higher VENC reduces the error caused by non-symmetric velocity distributions, and thus a tradeoff can be made between noise sensitivity and model dependency (figure 2).

Finite difference approximations of the IVSD are shown in figure 3 and are accompanied by PC-MRI IVSD mapping estimates. As in the case of velocity mapping, the assumption underlying IVSD mapping results in more robust estimations of the IVSD in presence of noise. For example, consider the upper right panel of figure 3 that shows the results of IVSD mapping with a Gaussian model performed on the velocity distribution in the upper left panel of figure 1. In spite of the distribution being clearly non-Gaussian, good accuracy was obtained for $\Delta k_v < 1$. Previously described guidelines for the choice of $\Delta k_v$ in IVSD mapping indicate that best IVSD sensitivity is obtained when $\Delta k_v = 1/\sigma_{opt}$, where $\sigma_{opt}$ is an IVSD value of interest such as the maximum expected (14). For this value of $\Delta k_v$, the error caused by the Gaussian assumption is less than 3% in the cases included here. For IVSD values lower than $\sigma_{opt}$ (or with a smaller $\Delta k_v$), the model dependency of the IVSD estimation declines.

Figure 4 shows results of finite difference approximations of the skew and kurtosis; as expected, a small $\Delta k_v$ results in accurate determination of these quantities. This demonstrates the potential of MRI to estimate these characteristics of the intravoxel velocity distribution. However, as for the lower order moments, the presence of noise markedly perturbs the estimates at small $\Delta k_v$, as this implies small differences in $S(k_v)$. Also, as expected, the accuracy of these finite difference approximations declines as the spacing $\Delta k_v$ increases.

Data describing the potential significance of the PC-MRI symmetry assumption for 2D through-plane velocity measurements are shown in table 2. With a VENC that matches the peak velocity and a spatial resolution of 7.5 pixels across the lumen diameter, the root-mean square velocity error was 0.06 m/s. Halving the VENC increased the error to 0.44 m/s and a two-fold increase in VENC reduced the error to 0.01 m/s, as predicted by the theory. The effect of the VENC on the root-mean-square error was similar at higher spatial resolutions.

## DISCUSSION

A generalized MRI framework for the quantification of any moment of arbitrary velocity distributions has been described. The moment framework is based on the fact that moments in the function domain (velocity space) correspond to derivatives in the Fourier transform domain ($k_v$-space) at $k_v = 0$. For proof of concept, moments of realistic velocity distributions were estimated by finite difference approximations of the derivatives of the MRI signal. In this way, the mean, standard deviation, skew, and kurtosis of the intravoxel velocity distribution were obtained. For the estimation of skew and kurtosis, a minimum of three steps in $k_v$-space are required, compared to two for mean velocity and IVSD. Estimation of these higher-order moments may thus be achieved with a dual-VENC PC-MRI acquisition that utilizes three different values of $|k_v|$ (16,17).

Being an integral part of the clinical evaluation of flow in many cardiovascular diseases (1), the applicability of PC-MRI velocity mapping is indisputable. IVSD mapping enables the estimation of turbulence intensity (11,12) and has potential for the estimation of wall shear stress (18). Applications of methods based on 3$^{rd}$ or higher order moments are yet to be evaluated. The estimation of the skew of $s(v)$, for example, could be used to assess the accuracy of PC-MRI velocity estimates.

As differences between measurements of $S(k_v)$ at $k_v$ close to zero with small $\Delta k_v$ (high VENC) become highly influenced by noise, determination of derivatives of $S(k_v)$ based on finite differentiation is challenging in practice and would require very high signal-to-noise ratio. The noise sensitivity increases by the order of differentiation, making skew and kurtosis estimates using finite differentiation impractical. By renouncing the requirement of validity for arbitrary distributions and introducing assumptions about the appearance of $s(v)$ more robust moment estimation approaches can be derived, as exemplified here by PC-MRI velocity and IVSD mapping (figures 2 and 3). In both PC-MRI velocity and IVSD mapping, the present results show that a smaller $\Delta k_v$ (higher VENC) yields estimates that are less impacted by the underlying assumptions (figures 2 and 3). The reason for this effect is that smaller values of $\Delta k_v$ lead to better approximations of the derivatives.

Flow rate calculations from PC-MRI velocity data are affected by the symmetry assumption (table 2). However, while the root-mean-square error of all pixel velocities in a slice is monotonically related to the VENC, the extent of the accumulated error in flow rate calculations is dependent on the appearance of the velocity field in combination with the spatial resolution. When accumulating velocities from several pixels in a slice, positive and negative errors cancel each other out to some extent and the resulting error in flow rate and volumetric flow may therefore be small, especially at higher spatial resolutions. However, the symmetry error can be expected to affect particle trace trajectories computed from 3D cine PC-MRI velocity data as these accumulate error over time; approaches for validation of such particle traces will be helpful in determining its significance (19).

Analysis of the derivatives of $S(k_v)$ has previously been used to address MRI motion estimation problems (18,20). Based on the derivatives of $S(k_v)$ and their interpretations, Pipe (18) derived the following expression for the estimation of the IVSD, which is valid for small values of $k_v$:

$$\sigma = \mathrm{sqrt}\left[\frac{2\left(1-|S(k_v)|/|S(0)|\right)}{k_v^2}\right] \text{ [m s}^{-1}\text{]} \qquad [16]$$

This expression, which can also be derived from the moment framework, yields IVSD estimates comparable to those obtained by finite differentiation. Similar to the case of PC-MRI velocity

mapping, an expression for the estimation of $\sigma$ that is valid for larger values of $k_v$ can be obtained by modeling a specific distribution of s($v$) and fitting the model parameters to measurements with larger $\Delta k_v$. If a Gaussian model is employed, which has been done for IVSD measurements in disturbed and turbulent flows, equation 3 is obtained (11,12). Further investigations are needed to design appropriate $s(v)$ models for the estimation of skew and kurtosis; such studies should also include real data and more detailed investigations on the impact of noise and eddy currents. The gradient strengths required for the estimation of skew and kurtosis are of the same order of magnitude as those used in PC-MRI velocity mapping and thus similar eddy current effects can be expected. Background phase offsets caused by such eddy currents would affect the estimation of skew and kurtosis; its significance may be reduced by post-processing. Further attention may also be needed regarding the fact that parts of the derivations in this study were based on Hermitian symmetry, which in practice would be affected by noise and phase errors due to inhomogeneities.

In conclusion, a framework for the quantification of any moment of arbitrary velocity distributions has been presented. This framework exploits that moments in velocity space correspond to derivatives in $k_v$-space. The framework proved to permit the estimation of the mean, standard deviation, skew, and kurtosis of the intravoxel velocity distribution. It furthermore facilitates improvements in the understanding and guidance of the application of current MRI moment estimation approaches, as demonstrated by an investigation of the significance of the symmetry assumption of PC-MRI velocity mapping. The symmetry assumption affects flow rate calculations and particle trace trajectories; its significance can be reduced by using a higher VENC.

## REFERENCES


1. Gatehouse PD, Keegan J, Crowe LA, Masood S, Mohiaddin RH, Kreitner KF, Firmin DN. Applications of phase-contrast flow and velocity imaging in cardiovascular MRI. Eur Radiol 2005;15(10):2172-2184.
2. Hahn E. Detection of sea-water motion by nuclear precession. Journal of Geophysical Research 1960;65(2):776-777.
3. van Dijk P. Direct cardiac NMR imaging of heart wall and blood flow velocity. Journal of computer assisted tomography 1984;8(3):429-436.
4. Bryant DJ, Payne JA, Firmin DN, Longmore DB. Measurement of flow with NMR imaging using a gradient pulse and phase difference technique. Journal of computer assisted tomography 1984;8(4):588-593.
5. O'Donnell M. NMR blood flow imaging using multiecho, phase contrast sequences. Medical Physics 1985;12(1):59-64.
6. Nayler GL, Firmin DN, Longmore DB. Blood flow imaging by cine magnetic resonance. Journal of computer assisted tomography 1986;10(5):715-722.
7. Axel L, Morton D. MR flow imaging by velocity-compensated/uncompensated difference images. Journal of computer assisted tomography 1987;11(1):31-34.
8. Moran PR. A flow velocity zeugmatographic interlace for NMR imaging in humans. Magnetic Resonance Imaging 1982;1(4):197-203.
9. Wolf RL, Ehman RL, Riederer SJ, Rossman PJ. Analysis of systematic and random error in MR volumetric flow measurements. Magn Reson Med 1993;30(1):82-91.
10. Hamilton CA, Moran PR, Santago P, Rajala SA. Effects of intravoxel velocity distributions on the accuracy of the phase-mapping method in phase-contrast MR angiography. Journal of Magnetic Resonance Imaging 1994;4(5):752-755.
11. Dyverfeldt P, Sigfridsson A, Kvitting JPE, Ebbers T. Quantification of intravoxel velocity standard deviation and turbulence intensity by generalizing phase-contrast MRI. Magn Reson Med 2006;56(4):850-858. [Erratum in: Magn Reson Med 2007;57(1):233]
12. Gao JH, Gore JC. Turbulent flow effects on NMR imaging: measurement of turbulent intensity. Medical Physics 1991;18(5):1045-1051.
13. Bracewell RN. The Fourier transform and its applications. New York: McGraw-Hill Companies, Inc.; 2000.

14. Dyverfeldt P, Gårdhagen R, Sigfridsson A, Karlsson M, Ebbers T. On MRI Turbulence Quantification. Magn Reson Imaging 2009;27(7):913-922.
15. Gårdhagen R, Lantz J, Carlsson F, Karlsson M. Quantifying Turbulent Wall Shear Stress In a Stenosed Pipe Using Large Eddy Simulation. J Biomech Eng 2010;132(6):061002.
16. Lee AT, Pike GB, Pelc NJ. Three-point phase-contrast velocity measurements with increased velocity-to-noise ratio. Magn Reson Med 1995;33(1):122-126.
17. Johnson KM, Markl M. Improved SNR in phase contrast velocimetry with five-point balanced flow encoding. Magnetic Resonance in Medicine 2010;63(2):349-355.
18. Pipe JG. A simple measure of flow disorder and wall shear stress in phase contrast MRI. Magnetic Resonance in Medicine 2003;49(3):543-550.
19. Eriksson J, Carlhäll CJ, Dyverfeldt P, Engvall J, Bolger AF, Ebbers T. Semi-automatic quantification of 4D left ventricular blood flow. Journal of Cardiovascular Magnetic Resonance 2010;12(1):9.
20. Tsai CM, Olcott EW, Nishimura DG. Flow quantification using low-spatial-resolution and low-velocity-resolution velocity images. Magnetic Resonance in Medicine 1999;42(4):682-690.

LIST OF TABLES

*Table 1. Examples of moments of a distribution*

| Moment | Interpretation [a] |
|---|---|
| First raw moment, $\mu'_1$ | Mean, $V = \mu'_1$ |
| Second central moment, $\mu_2$ | Standard deviation, $\sigma = \mathrm{sqrt}(\mu_2)$ |
| Third central moment [b], $\mu_3$ | Skew, $\gamma_1 = \mu_3/\sigma^3$ |
| Fourth central moment [b], $\mu_4$ | Kurtosis, $\gamma_2 = \mu_4/\sigma^4$ |

[a] For a non-normalized distribution, these quantities are obtained by normalization of the moment with the zeroth moment of the distribution.

[b] Also known as the 3rd and 4th standardized moments, respectively.

*Table 2. Error in PC-MRI velocity data resulting from the symmetry assumption. 2D PC-MRI velocity measurements were simulated from post-stenotic numerical velocity data that had a peak jet velocity of about 7 m/s. Errors are shown for different combinations of VENC and pixel size.*

| | Pixel size = 1x1 $mm^2$ (~15 pixels across lumen diameter) | Pixel size = 1.5x1.5 $mm^2$ (~10 pixels across lumen diameter) | Pixel size = 2x2 $mm^2$ (~7 pixels across lumen diameter) |
|---|---|---|---|
| VENC = 3.5 m/s | PE = 0.08 %<br>RMSE = 0.22 m/s | PE = 0.05 %<br>RMSE = 0.27 m/s | PE = 4.16 %<br>RMSE = 0.44 m/s |
| VENC = 7 m/s | PE = 0.04 %<br>RMSE = 0.03 m/s | PE = 0.21 %<br>RMSE = 0.05 m/s | PE = 0.13 %<br>RMSE = 0.06 m/s |
| VENC = 14 m/s | PE = 0.01 %<br>RMSE = 0.01 m/s | PE = 0.07 %<br>RMSE = 0.01 m/s | PE = 0.01 %<br>RMSE = 0.01 m/s |

PE = percentage error in flow rate calculation from PC-MRI velocity data

RMSE = Root-mean-square error of PC-MRI velocities

LIST OF FIGURE CAPTIONS

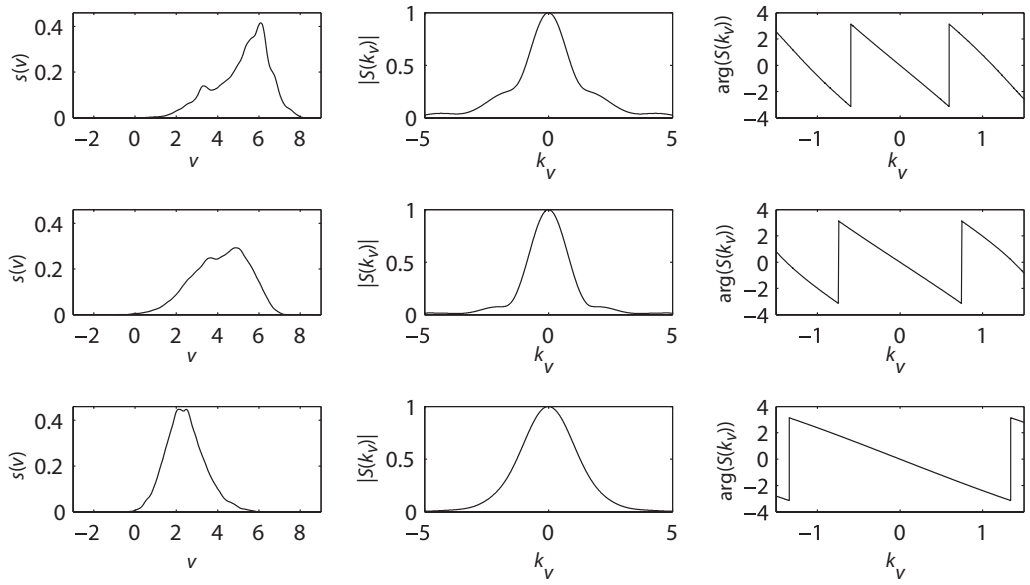


Figure 1. Left column: Three different spin velocity distributions s($v$) along with the modulus (middle column) and the argument (right column) of the corresponding MRI signal $S(k_v)$. Each row represents results from one voxel of the simulated data. Note that because the velocity distributions are not symmetric, arg($S(k_v)$) are not linearly related to $k_v$; this is just about detectable in the plots.

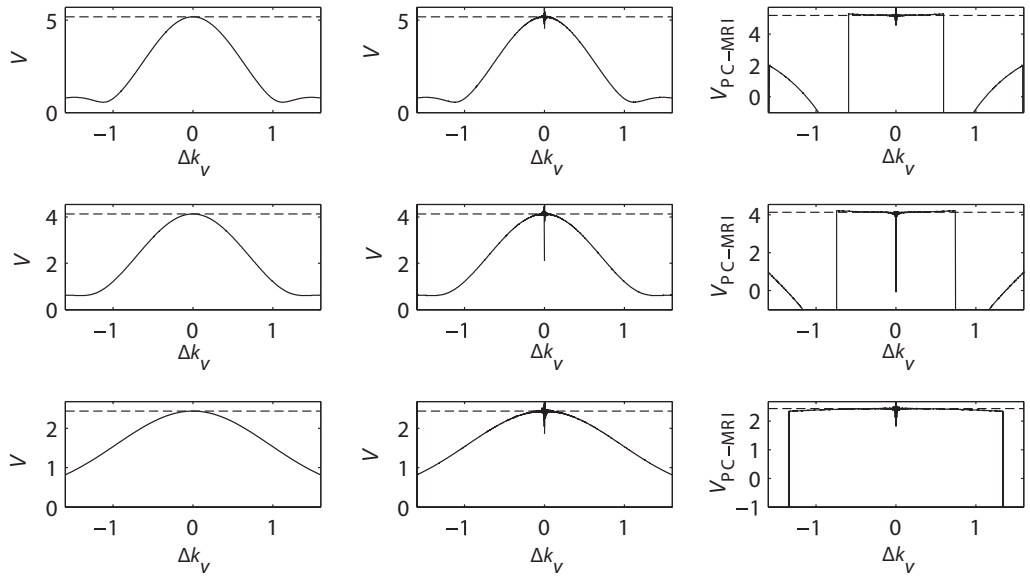


Figure 2. Estimations of the first raw moment (mean velocity) of the distributions in figure 1. The mean of $s(v)$, $V$, as obtained by finite difference approximations of the first derivative of $S(k_v)$ at $k_v = 0$ in absence of noise (left column), presence of noise (middle column), and as obtained by the PC-MRI phase-difference method (right column). The dashed lines indicate the true $V$. On the interval $|\Delta k_v| < \pi / V$ , the deviations of the PC-MRI estimates from the true $V$ are due to the assumption that $s(v)$ is a symmetric distribution. At $|\Delta k_v| > \pi / V$, velocity aliasing occurs. Each row represents results from one voxel.

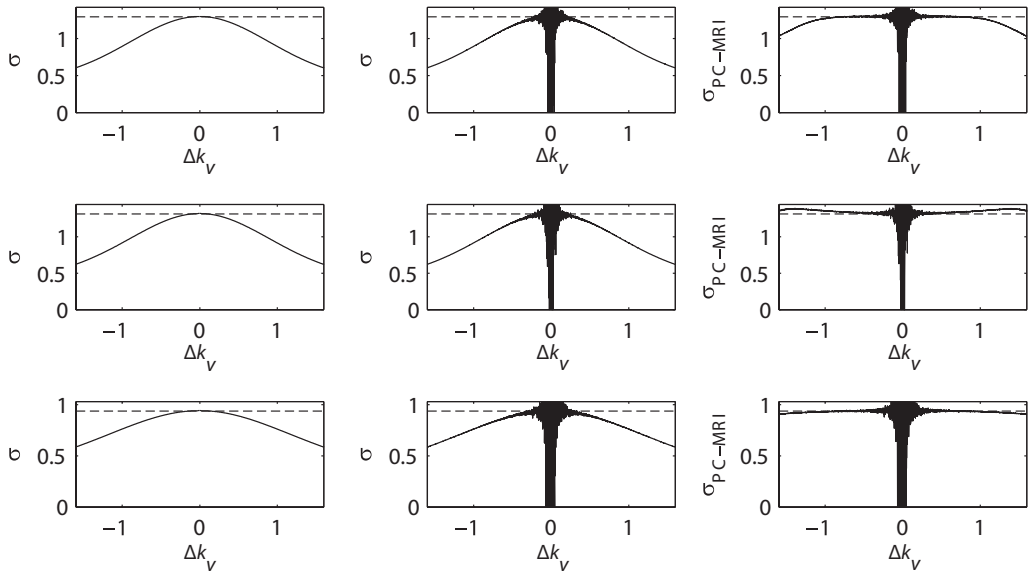


Figure 3. Estimations of the second central moment (IVSD) of the distributions in figure 1. The standard deviation of $s(v)$, σ, as obtained by finite difference approximations of the second derivative of $S(k_v)$ at $k_v = 0$ in absence of noise (left column), presence of noise (middle column), and as obtained by the PC-MRI IVSD method (right column). The dashed lines indicate the true σ. In c), the deviations of the PC-MRI estimates from the true σ are due to the assumption that $s(v)$ is a Gaussian distribution. Each row represents results from one voxel.

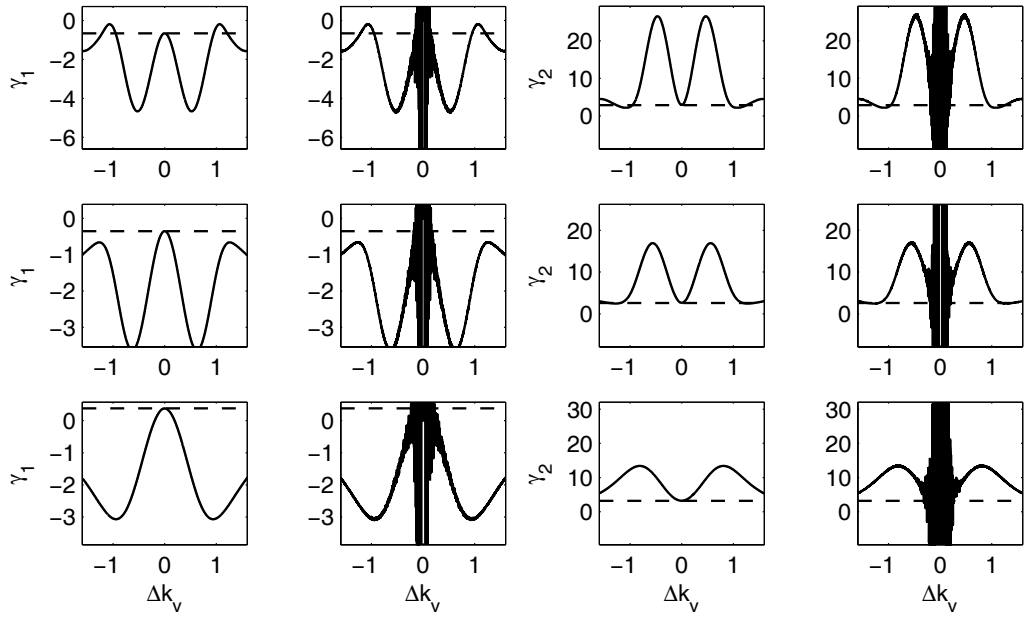


Figure 4. Estimations of the skew ($\gamma_1$) and kurtosis ($\gamma_2$) of the distributions in figure 1. The skew estimated in absence and presence of noise is shown in the first and second column, respectively. The third and fourth columns contain the corresponding results for kurtosis. The dashed lines indicate the true values. Each row represents results from one voxel. The true values for $\gamma_1$ and $\gamma_2$ are for the first row: -0.7 and 2.9, second row: -0.4 and 2.6, third row: 0.4 and 3.2. For comparison, with the definitions used here (table 1), $\gamma_1$ and $\gamma_2$ for a normal distribution is 0 and 3, respectively.